

UC Santa Barbara

UC Santa Barbara Previously Published Works

Title

Exploring Mission Design for Imaging Spectroscopy Retrievals for Land and Aquatic Ecosystems

Permalink

<https://escholarship.org/uc/item/3vt647kr>

Journal

Journal of Geophysical Research Biogeosciences, 128(4)

ISSN

2169-8953

Authors

Raiho, AM
Cawse-Nicholson, K
Chlus, A
[et al.](#)

Publication Date

2023-04-01

DOI

10.1029/2022jg006833

Copyright Information

This work is made available under the terms of a Creative Commons Attribution License, available at <https://creativecommons.org/licenses/by/4.0/>

Peer reviewed

JGR Biogeosciences

RESEARCH ARTICLE

10.1029/2022JG006833

Special Section:

The Earth in living color: spectroscopic and thermal imaging of the Earth: NASA's Decadal Survey Surface Biology and Geology Designated Observable

Key Points:

- High spectral resolution (~10 nm), high spatial resolution (~30 m), and high revisit (less than 16 days) is needed to estimate Earth's geophysical properties with imaging spectroscopy and corresponding retrieval algorithms
- We simulate the effects of instrument signal-to-noise ratios on retrieval accuracy using a codebase called Hypertrace
- Our approach provides a framework for current and future mission design planning to improve geophysical property estimation accuracy across biogeoscience

Correspondence to:

A. M. Raiho,
ann.m.raiho@nasa.gov

Citation:

Raiho, A. M., Cawse-Nicholson, K., Chlus, A., Dozier, J., Gierach, M., Miner, K., et al. (2023). Exploring mission design for imaging spectroscopy retrievals for land and aquatic ecosystems. *Journal of Geophysical Research: Biogeosciences*, 128, e2022JG006833. <https://doi.org/10.1029/2022JG006833>

Received 15 FEB 2022

Accepted 4 OCT 2022









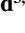


Author Contributions:

Conceptualization: A. M. Raiho, K. Cawse-Nicholson, A. Chlus, J. Dozier, M. Gierach, K. Miner, F. Schneider, D. Schimel, S. Serbin, A. N. Shiklomanov, D. R. Thompson, P. A. Townsend, S. Zareh, M. Skiles, B. Poulter

Data curation: K. Cawse-Nicholson, J. Dozier, M. Gierach, K. Miner, F. Schneider, D. Schimel, D. R. Thompson, P. A. Townsend, S. Zareh, M. Skiles, B. Poulter

Formal analysis: A. M. Raiho, S. Zareh, M. Skiles

Exploring Mission Design for Imaging Spectroscopy Retrievals for Land and Aquatic Ecosystems

A. M. Raiho^{1,2} , K. Cawse-Nicholson³ , A. Chlus³, J. Dozier⁴ , M. Gierach³ , K. Miner³, F. Schneider³ , D. Schimel³, S. Serbin⁵ , A. N. Shiklomanov¹ , D. R. Thompson³ , P. A. Townsend^{3,6} , S. Zareh³, M. Skiles⁷ , and B. Poulter¹ 

¹NASA Goddard Space Flight Center, Biospheric Sciences Lab, Greenbelt, MD, USA, ²Earth System Science Interdisciplinary Center, University of Maryland, College Park, MD, USA, ³Jet Propulsion Laboratory, California Institute of Technology, Pasadena, CA, USA, ⁴Bren School of Environmental Science & Management, University of California, Santa Barbara, CA, USA, ⁵Brookhaven National Laboratory, Upton, NY, USA, ⁶University of Wisconsin—Department of Forest and Wildlife Ecology, Madison, WI, USA, ⁷Department of Geography, University of Utah, Salt Lake City, UT, USA

Abstract The retrieval algorithms used for optical remote sensing satellite data to estimate Earth's geophysical properties have specific requirements for spatial resolution, temporal revisit, spectral range and resolution, and instrument signal-to-noise ratio (SNR) performance to meet biogeoscience objectives. Studies to estimate surface properties from hyperspectral data use a range of algorithms sensitive to various sources of spectroscopic uncertainty, which are in turn influenced by mission architecture choices. Retrieval algorithms vary across scientific fields and may be more or less sensitive to mission architecture choices that affect spectral, spatial, or temporal resolutions and spectrometer SNR. We used representative remote sensing algorithms across terrestrial and aquatic study domains to inform aspects of mission design that are most important for impacting accuracy in each scientific area. We simulated the propagation of uncertainties in the retrieval process including the effects of different instrument configuration choices. We found that retrieval accuracy and information content degrade consistently at >10 nm spectral resolution, >30 m spatial resolution, and >8-day revisit. In these studies, the noise reduction associated with lower spatial resolution improved accuracy vis à vis high spatial resolution measurements. The interplay between spatial resolution, temporal revisit, and SNR can be quantitatively assessed for imaging spectroscopy missions and used to identify key components of algorithm performance and mission observing criteria.

Plain Language Summary Detailed observations of Earth's visible to shortwave infrared spectra, known as hyperspectral imagery or imaging spectroscopy, will provide novel insights across scientific disciplines. Vegetation, aquatic, mineral, and snow scientists have independently developed techniques for using hyperspectral imagery to measure different features of their targets. But developing measurement objectives that will work well for every kind of measurement target is difficult. Here, we test several representative image analysis techniques to inform the planning process of future hyperspectral missions. Specifically, we investigate the effect that changing the number of spectral bands, the size of image pixels, and the frequency of repeat observations has on each technique's accuracy.

1. Introduction

Light reflected from the Earth's surface provides information on the chemical processes and their constituents in land, aquatic and oceanic systems. Vegetation both absorbs and reflects light as a function of photosynthesis, water and nutrient status, mineral surfaces reflect light based on their composition of various elements, and aquatic systems reflect water-leaving radiances that are linked to surface and column-water features. Combined, reflectances and their derived properties have informed the study of the Earth's biogeochemistry, biodiversity, climate system and how it is changing due to human activities. Satellite missions, launched since the late 1970s, provide a now continuous time series of global change, with information on vegetation greenness, disturbance, algal blooms, landslides, informing a wide-array of science and applications. Presently, an emergence of new instruments to observe reflectance using imaging spectroscopy will further broaden and deepen the insights retrieved on the Earth system and functioning.

Global imaging spectroscopy from NASA's Surface Biology and Geology (SBG) designated observable will improve understanding of five focal areas of biogeoscience: marine and terrestrial ecosystems, seasonal to

Funding acquisition: K. Cawse-Nicholson, A. Chlus, J. Dozier, M. Gierach, F. Schneider, D. Schimel, S. Serbin, A. N. Shiklomanov, P. A. Townsend, B. Poulter

Investigation: A. M. Raiho, K. Cawse-Nicholson, M. Gierach, K. Miner, F. Schneider, D. Schimel, S. Serbin, D. R. Thompson

Methodology: A. M. Raiho, K. Cawse-Nicholson, A. Chlus, J. Dozier, M. Gierach, F. Schneider, D. Schimel, S. Serbin, A. N. Shiklomanov, D. R. Thompson, P. A. Townsend, S. Zareh, M. Skiles, B. Poulter

Project Administration: K. Cawse-Nicholson, A. Chlus, J. Dozier, M. Gierach, K. Miner, F. Schneider, D. Schimel, S. Serbin, A. N. Shiklomanov, P. A. Townsend, B. Poulter

Resources: K. Miner, D. Schimel, S. Serbin

Software: A. M. Raiho, A. Chlus, J. Dozier, M. Gierach, D. Schimel, S. Serbin, A. N. Shiklomanov, D. R. Thompson, P. A. Townsend, S. Zareh, M. Skiles, B. Poulter

Supervision: K. Cawse-Nicholson, A. Chlus, J. Dozier, M. Gierach, D. Schimel, S. Serbin, A. N. Shiklomanov, P. A. Townsend, B. Poulter

Validation: A. M. Raiho

Visualization: A. M. Raiho, A. Chlus, F. Schneider, D. Schimel, A. N. Shiklomanov, D. R. Thompson

Writing – original draft: A. M. Raiho, K. Cawse-Nicholson, J. Dozier, D. Schimel, S. Serbin, A. N. Shiklomanov, S. Zareh, M. Skiles, B. Poulter

Writing – review & editing: A. M. Raiho, K. Cawse-Nicholson, A. Chlus, J. Dozier, M. Gierach, K. Miner, F. Schneider, D. Schimel, S. Serbin, A. N. Shiklomanov, D. R. Thompson, P. A. Townsend, S. Zareh, M. Skiles, B. Poulter

centennial climate variability, weather and air quality, hydrology and water resources, and dynamics and hazards associated with Earth's surface and interior (National Academies of Sciences, Engineering, and Medicine, 2018; Schimel et al., 2020). SBG will provide visible through shortwave-infrared reflectance (~380–2,500 nm wavelengths) and thermal (4.5–12 μm) emissivity observations from space with global coverage, frequent revisit, and high spectral fidelity (Stavros et al., 2023). Designing a successful mission that meets diverse scientific objectives requires evaluating alternative mission architectures (Stavros et al., 2023; Thompson et al., 2021). In SGB's case, each science focal area depends on a different aspect of mission architecture for accuracy (Cawse-Nicholson et al., 2021). To characterize the scientific impact of trade-offs associated with different mission architectures, we illustrate the driving examples behind each focal area (Table 1) and assess the effects of measurement trades on a target retrieval.

Trade-offs are a fundamental component of mission design. Fundamental trade-offs associated with different mission architectures occur between spectral, spatial, and temporal resolutions and the radiometric precision of the instrument. Radiometric precision (i.e., signal-to-noise ratio or SNR) is a function of the number of photons an instrument receives. When integrating over a smaller spectral (i.e., higher spectral resolution) or spatial area (i.e., higher spatial resolution) at the fixed orbital speed of a spacecraft, fewer photons will reach the instrument, degrading SNR with downstream consequences for retrievals of geophysical variables. On the other hand, some features of interest require fine spectral and spatial resolution to be accurately retrieved. Mission architecture design must address how optimizing for high instrument SNR impacts spectral, spatial, and temporal resolution. For a mission like SBG, which covers a range of scientific disciplines, the trades between each of the three types of resolutions and SNR must be thoroughly evaluated using a consistent traceability framework.

Imaging spectroscopy (i.e., 100–1,000s of contiguous wavelength channels) allows for more precise discrimination of Earth surface properties than multispectral imagery (i.e., 3–20 wavelength channels) because of the higher information content in these hyperspectral measurements (Cawse-Nicholson et al., 2019; Thompson, Boardman, et al., 2017). The spectral resolution of a hyperspectral image has been shown to greatly affect mineral (Swayze, 2003) and vegetation (Shiklomanov et al., 2016) retrieval accuracy because these algorithms require fine spectrally resolved information. Here, we define “algorithm” similarly to Cawse-Nicholson et al. (2021) as a method used to derive an Earth surface property of interest from remotely sensed data. In both these cases, high spectral resolution may compensate for lower SNR by contributing more information content. Requirements also vary considerably by algorithm type. For example, snow retrieval algorithms are like common mineral retrieval algorithms that consider the spectral signature around known absorption wavelengths (Nolin & Dozier, 1993). As such, a stronger focus on fine spectral resolution is needed to discriminate and identify key mineral absorption features associated with specific mineral species or to identify or discriminate dust versus snow grain particles, as well as determine water content and age of snowpack (Swayze, 2003). On the other hand, vegetation algorithms are typically based on statistical models (e.g., Partial Least Squares Regression, PLSR; Burnett et al., 2021) or physically based models (e.g., radiative transfer model inversion) that relate plant properties at leaf or canopy level to more broad absorption features (e.g., Curran, 1989) and spectral information (Serbin & Townsend, 2020; Verrelst et al., 2019). As such, vegetation algorithms tend to require relatively higher SNR or spatial resolution over very fine spectral resolution (i.e., <10 nm) compared to the other science areas for reliable vegetation retrievals. Aquatic algorithms are especially sensitive to atmospheric noise in the spectral signal, and their retrieval accuracy may be particularly susceptible to degrading spectral resolution and the effects of low SNR because of how aquatic properties such as glint (Hu, 2011), bubbles (Dierssen, 2021), and optical variability in the water column (Garcia et al., 2020) interact with water-leaving radiances. In our analyses, we demonstrate how retrieval algorithms that depend on hyperspectral imagery respond to the effects of degrading spectral resolution and radiometric precision on retrieval accuracy.

Holding SNR constant, finer spatial resolution or increased number of pixels per image will typically lead to higher information content in an image (Cawse-Nicholson et al., 2019). However, instrument SNR decreases with finer spatial resolution because smaller pixels result in fewer photons received by each focal plane array detector element. A driving case for spatial resolution is the ecological focal area where different ecosystems have different dominating spatial scale processes (Turner et al., 1989; Wang et al., 2018). For instance, a homogenous scene (e.g., dense deciduous forest) may not require fine spatial detail to understand plant functional traits while a heterogeneous scene (e.g., sparse lower montane ecosystem) with a variety of landscape classifications and vegetation community types may require fine spatial detail.

Table 1
Experiment List

Resolution	Core science area (scene)	Algorithm	L3 retrieval (units)
Spectral	Mineral (Cuprite, Nevada, USA; AVIRIS-C; Swayze et al., 2014)	Absorption feature matching	Mineral mass fraction (unitless; i.e., spectral abundance)
	Aquatic (Arlington, Great Barrier Reef, Australia; DESIS; German Aerospace Center, 2019)	Benthic cover classifier	Benthic cover type (unitless)
	Vegetation (Western Ghats, South India; Zheng et al., 2023)	Partial least squares regression	Leaf nitrogen mass fraction (g/mg)
	Snow (Southern Rocky Mountains, USA; Skiles & Painter, 2017)	Least squares	Snow grain size (μm)
Spatial	Vegetation (Western Ghats, South India; Zheng et al., 2023)	Partial least squares regression	Leaf nitrogen mass fraction (g/mg)
	Vegetation (Crested Butte, Colorado, USA; Chadwick et al., 2020)	Partial least squares regression	Leaf nitrogen mass fraction (g/mg)
Temporal	Event detection (Simulation)	NA	Event (no units)

Note. Each row describes the components of an experiment in our study grouped by the trade study resolution of interest. If citations are applicable, they are found in parentheses.

Frequent temporal revisit is another fundamental aspect of mission architecture and provides a basis for quantifying the effects of natural disasters and seasonal phenomena (Schimel et al., 2020). The ability to detect a short-duration event (e.g., a volcanic eruption or mudslide) or frequent changes during a season (e.g., snow albedo) may be hindered by longer revisit time intervals, areas where cloud cover is common, or by overpass time. However, increasing revisit frequency can be obtained at the cost of spatial resolution and must be quantitatively justified.

To optimize for retrieval accuracy across five scientific areas, mission architecture design must consider tradeoffs between spectral, spatial, and temporal resolutions. In this study, we look at specific driving case studies to quantify the performance impacts of these design choices on the range of SBG science objectives. Specifically, we perform a simulation experiment in which we synthesize artificial imaging spectroscopy data and apply state of practice retrieval algorithms with varying sensor noise and resolution. Currently, high resolution hyperspectral time series data are uncommon, so our strategy is to show the probability of detecting an event depending on event duration and revisit time interval using simulated data. Our approach compares algorithm accuracy with and without instrument noise along gradients of coarsening resolutions to determine optimal resolutions for imaging spectroscopy architecture design.

2. Materials and Methods

Radiance measurements from hyperspectral missions will be converted into surface reflectance values through atmospheric correction, which isolates and removes the contribution of absorption and scattering from atmospheric aerosols, water vapor, and other components on the overall radiance signal, and provides estimates of incoming and outgoing radiation for each pixel at the Earth surface (Vermote & Kotchenova, 2008). In this study, we use an atmospheric correction approach that employs a physically based atmospheric radiative transfer model inversion. We use the Imaging Spectrometer Optimal FITting codebase (i.e., ISOFIT; Thompson et al., 2018), whereby atmospheric and surface reflectance can be estimated jointly using optimal estimation (OE; Thompson et al., 2018). Estimated surface reflectance from the OE procedure then provides the information for algorithms that retrieve geophysical properties. These algorithms can take many forms. The retrieval algorithms listed in Table 1 were chosen to span each of the five core scientific areas chosen in the decadal survey and were made available through collaborations with the algorithms working group.

2.1. Hypertrace and Instrument Modeling

We developed the Hypertrace simulation workflow to trace the hyperspectral data uncertainty pipeline from top of atmosphere radiance to bio- and geophysical retrievals (<https://github.com/isofit/isofit/tree/master/examples/py-hypertrace>). Operationally, Hypertrace starts from known surface reflectance and atmospheric conditions based on a specific spectral resolution, and then simulates top-of-atmosphere radiance and instrument radiances based on the proposed instrument design, and then performs atmospheric correction via optimal estimation to

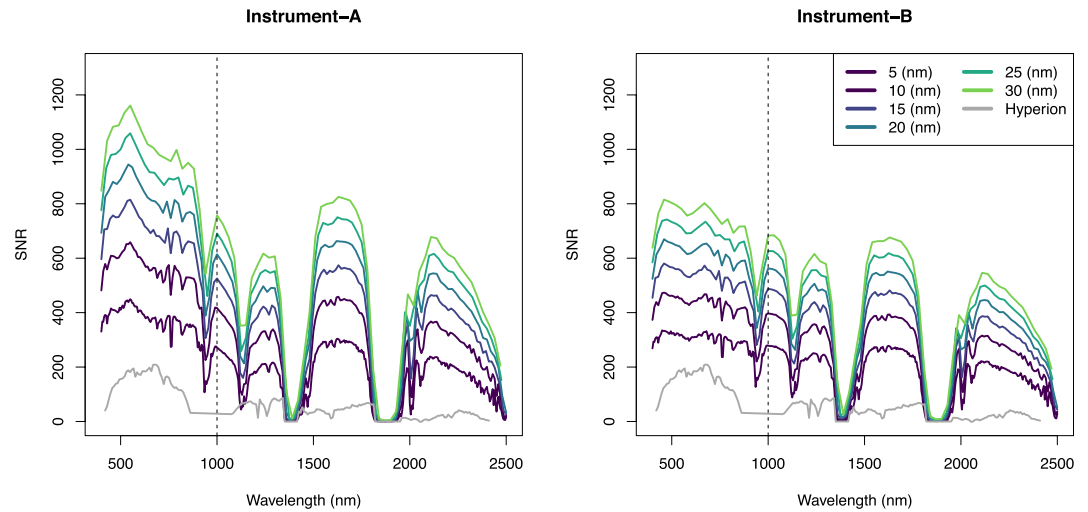


Figure 1. Instrument SNR over the visible and near-infrared (VNIR; 400–1,000 nm) and short wave infrared (SWIR; 1,000–2,500 nm) for Instrument-A (left) and Instrument-B (right) spectrometers colored by spectral resolution (nm) range considered in this study. The vertical line in each panel represents the split between the VNIR and the SWIR.

estimate surface reflectance. Pragmatically, Hypertrace is a wrapper around the ISOFIT codebase (see Isofit et al., 2021) which provides both forward and inverse reflectance modeling for translation between reflectance and radiance. Our ISOFIT configuration files can be found in the supplemental materials. Hypertrace manages this simulation process at runtime, and applies geophysical retrieval algorithms to the estimated surface reflectance. Hypertrace is written in Python and can be configured with a simple JSON interface.

Hypertrace allows for the inclusion of different imaging spectrometer detector configurations that provide various SNR profiles (Figure 1). An imaging spectrometer includes the optical system and the detector. The optics include the telescope, a dispersive element such as a prism or diffraction grating, and the slit, the entrance width that determines photon throughput. In our experiments, we used configurations for two Chroma instruments (i.e., focal plane array) Instrument-A and Instrument-B detectors and also Hyperion, where Instrument-A has a detector pixel pitch of 0.0030 cm and a slit width of 30 microns while Instrument-B has a detector pixel pitch of 0.0018 cm and a slit width of 18 microns. We selected these Chroma spectrometers as examples because they have been used in the Earth Surface Mineral Dust Source Investigation (EMIT) mission, a similar imaging spectroscopy mission to SBG (Connelly et al., 2021). We compare against Hyperion to show the abilities of our workflow to include SNR from both future and past instruments. These spectrometer settings as well as desired instrument spatial resolution alter the SNR along the visible to shortwave infrared (Figure 1).

For the Chroma instruments, we derived instrument SNR using the following approach. The SNR describes the ratio of the signal to noise for the given spatial resolution element, where the signal is defined as the total number of collected electrons per unit area (i.e., pixel) over the total noise for the same area. The signal is proportional to the following equation:

$$\text{Signal} = L * \delta\lambda * A_o * \Omega_d * t_{\text{int}} * T * \eta \quad (1)$$

where L is spectral radiance at sensor, $\delta\lambda$ is the detector element's spectral response, A_o is the instrument telescope aperture, Ω_d is the solid angle of the instrument, t_{int} is the integration time per spatial sample, T is transmission of the instrument, combining all lenses, filters, mirrors and gratings in the primary optical path, and η is the detector quantum efficiency.

For a given spatial sample, the noise comes from multiple contributing factors, including the shot noise, dark noise, read noise, electronics noise, and quantum noise.

$$\text{Noise} = \sqrt{N_{\text{shot}}^2 + N_{\text{dark}}^2 + N_{\text{read}}^2 + N_{\text{electronics}}^2} \quad (2)$$

The shot noise is usually the largest contributor to the noise and is a Poissonian effect that is an inherent property of the photon collection phenomenon in optical devices. The dark noise is the product of the dark current

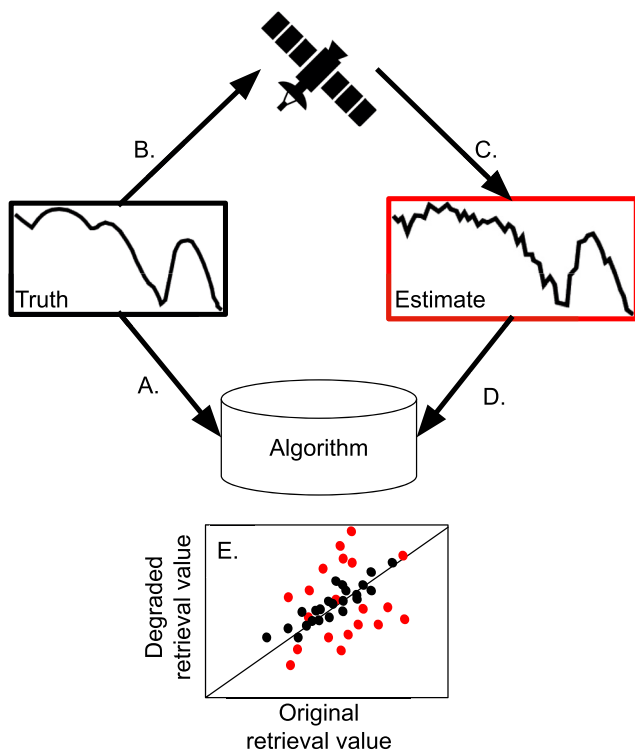


Figure 2. Conceptual diagram of one iteration of our analysis. (a) True surface reflectance is used to obtain true or direct retrievals that are not affected by the noise (black). (b) and (c) True surface reflectance is run through hypertrace forward (b) and inverse (c) models to obtain estimated surface reflectance including uncertainties from atmospheric correction and instrument design signal-to-noise ratio. (d) These estimated reflectances (red) are given to the same algorithms and then compared to the directly estimated retrievals (e).

of the focal plane array and the integration times we work with. The read noise is associated with every frame read. For digital focal plane array like Instrument-B the electronics noise is zero while it is a non-zero value for the analog version Instrument-A. Usually the focal plane array gets characterized in a laboratory thermal-vacuum chamber that allows the read noise, dark current, well capacity, linearity, and crosstalk to be measured and characterized. The results of these characterizations are critical to the design and performance predictions of imaging spectrometers using the focal plane array.

For the Hyperion instrument, we used a parametric approach for calculating instrument SNR. First, we collected invariant scenes from early in the Hyperion campaign. We then used the radiance from the invariant scenes and the parameter noise estimation process from Bioucas-Dias and Nascimento (2005) to derive SNR for Hyperion.

2.2. Spectral and Spatial Sensitivity

Our simulation experiments have two parts: In “direct” experiments, we apply retrieval algorithms to degraded reflectance data, and compare the outcome to a similar retrieval at native resolution (Figure 2, black). In “instrument” experiments, we degrade the radiance at sensor in Hypertrace using an instrument model, perform an atmospheric correction, and then apply the retrieval algorithm to the estimated surface reflectance. Therefore, only the instrument experiments include the effect of imperfect instrument radiometry (“noise”). We illustrate the concept behind our simulations in Figure 2. In the “instrument” experiments, we consider two instrument models, representing state-of-the-art detectors due to launch in the near future (EMIT, Connelly et al., 2021). We use Hypertrace to simulate the contributions of imperfect radiometry in Instrument-A, Instrument-B, or Hyperion spectrometer to biases and uncertainties in the geophysical variable of interest (Figure 2, red). We repeat the direct and instrument application steps along the resolution degradation range of interest. We then compare both the direct retrievals and

the Hypertrace retrievals to the direct retrieval at the native resolution using a variety of standard validation statistics, for example, root mean square error (RMSE) and kappa score (for categorical data) to illustrate the effects of degrading resolution on retrieval accuracy.

We chose spectral and spatial resolution experiments to demonstrate accuracy degradation across the full range of current mission design choices and corresponding trades with SNR. In our spectral resolution experiments, we varied the bandwidth from 5 to 30 nm in 5 nm increments, resulting in 6 experiments with a minimum of 70 bands and a maximum of 421 bands. Similarly, we varied spatial resolution from 20 to 60 m by 10 m increments. We also included 100 m spatial resolution experiments to demonstrate algorithm accuracy at very low spatial resolutions. The scenes were resampled to coarser resolutions using Gaussian convolution aggregation for spectral resolution and bilinear averaging for spatial resolution (ignoring potential autocorrelation between spectral bands). We then repeated these experiments including the corresponding effects of SNR shown in Figure 1 (See Figure 2, black vs. red). All experiments were conducted with 1,000 randomly drawn points from each scene.

We chose representative hyperspectral scenes listed in Table 1 column 2 based on a set of science areas where retrieval algorithms were available and provided by the algorithm developers. These scenes have been bidirectional reflectance distribution function (BRDF) corrected and atmospherically corrected, meaning they provide estimates of the hemispherical-directional reflectance factor (HDRF, *sensu* Schaepman-Strub et al., 2006) for a nadir viewing angle. Table 1 lists the supporting citations for each scene.

The algorithms use a variety of methods. Absorption feature matching uses specific features of the reflectance spectrum and measures the depth of the feature to approximate the amount of the mineral present (Swayze et al., 2003). Benthic reflectance inversion (Thompson, Hochberg, et al., 2017) and benthic cover classifier

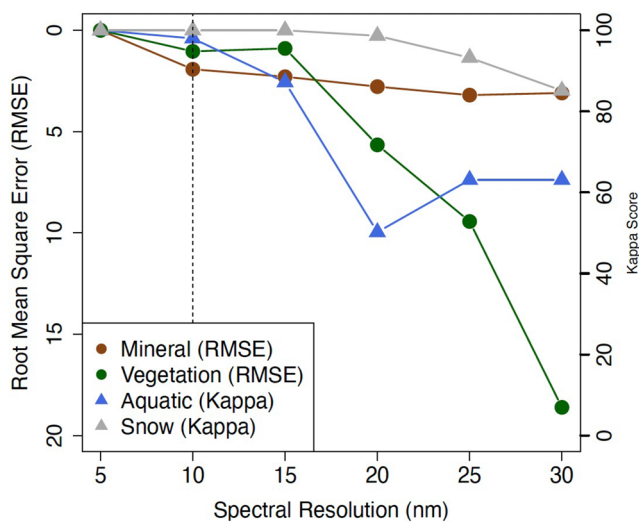


Figure 3. Direct application algorithm accuracy across spectral resolution colored by scientific area. These retrievals were calculated using true reflectance and each of the retrieval algorithms. Root mean square error was calculated for mineral and vegetation spectra while kappa score was calculated for aquatic and snow spectra. Vertical lines represent spectral resolution targets defined by the National Academies' 2017 Decadal Survey on Earth Science and Applications.

(Hochberg and Atkinson, 2003) which we refer to together as ‘benthic cover classifier’ and least squares (Dozier & Painter, 2004) approaches rely on in situ data to determine which benthic cover type or snow grain size a particular reflectance represents. PLSR also uses in situ data to derive coefficients that are then applied to the reflectance to retrieve a vegetation property (e.g., leaf nitrogen mass fraction).

2.3. Temporal Revisit

Acquisitions with high temporal revisit for hyperspectral data are rare in airborne (i.e., AVIRIS-NG) and spaceborne archives, including PRISMA and DESIS. Lack of high revisit hyperspectral data is problematic for assessing algorithm performance and expected event detection efficiency (Schimel et al., 2020). To overcome this obstacle here to provide quantitative information for mission architecture design in terms of revisit, we use an analytical approach where we calculate event detection probability (θ) by dividing event duration (γ) by the revisit interval (dt) such that,

$$\theta = \frac{\gamma}{dt} \quad (3)$$

We calculated θ across event durations 1–58 days and revisit intervals between 1 and 70 days and plotted θ as functions over increasing revisit interval. The analytical study quantifies the amount of information missed by decreasing temporal resolution (dt) for disturbance events with short event durations such as fires, volcanic eruptions or landslides, which have been listed as SBG designated observables (National Academies of Sciences, Engineering, and Medicine, 2018).

Satellite constellations have been proposed to increase revisit time intervals by increasing the number of instruments. We provide a brief analysis of uncertainty in a vegetation retrieval caused by instrument calibration drift. Calibration drift is the time between instrument calibration at an invariant site where the longer the time the more uncertainty from drift can be expected. For this analysis, we use calibration drift uncertainty estimates derived from AVIRIS-NG where we took a random draw from a multivariate normal with mean zero and covariance from the AVIRIS-NG estimate. We applied this draw linearly to a single radiance vector to represent how drift may increase uncertainty over time. From this set of radiances with increasing drift, we estimated surface reflectance using an ISOFIT inversion. Finally, we calculated the canopy nitrogen content in the set of estimated reflectances using PLSR and compared the nitrogen estimates over days since calibration by calculating the relative error percentage.

3. Results

3.1. Spectral Resolution

High spectral resolution (<20 nm) resulted in greater algorithm accuracy across all scientific areas in the direct algorithm application (Figure 3). The 10 nm standard proposed by NASA Earth Sciences Decadal Survey (2018) provided the algorithm accuracy across experiments (Figure 3, vertical dotted line). On average, vegetation PLSR was the most sensitive to spectral resolution degradation, with an average RMSE change of 1.7 between experiments followed by the least squares snow grain size retrieval and the aquatic benthic cover classifier with an average of -8.78 and -7.38 change in kappa score respectively. Least squares (i.e., snow) appears to be the least sensitive to spectral resolution degradation.

Accuracy was not degraded significantly with the inclusion of instrument noise for the mineral or aquatic spectral resolution experiments (Figure 4). Both Instrument-A and Instrument-B had increased retrieval accuracy between 5 and 10 nm because of the tradeoffs between SNR and spectral resolution (Figure 4a). The vegetation retrievals were similar across spectral resolutions for Instrument-A and Instrument-B. However, Hyperion performed poorly (i.e., RMSE = 23.54 mg/g; Figure 4b). The benthic cover classifier for the aquatic spectral resolution

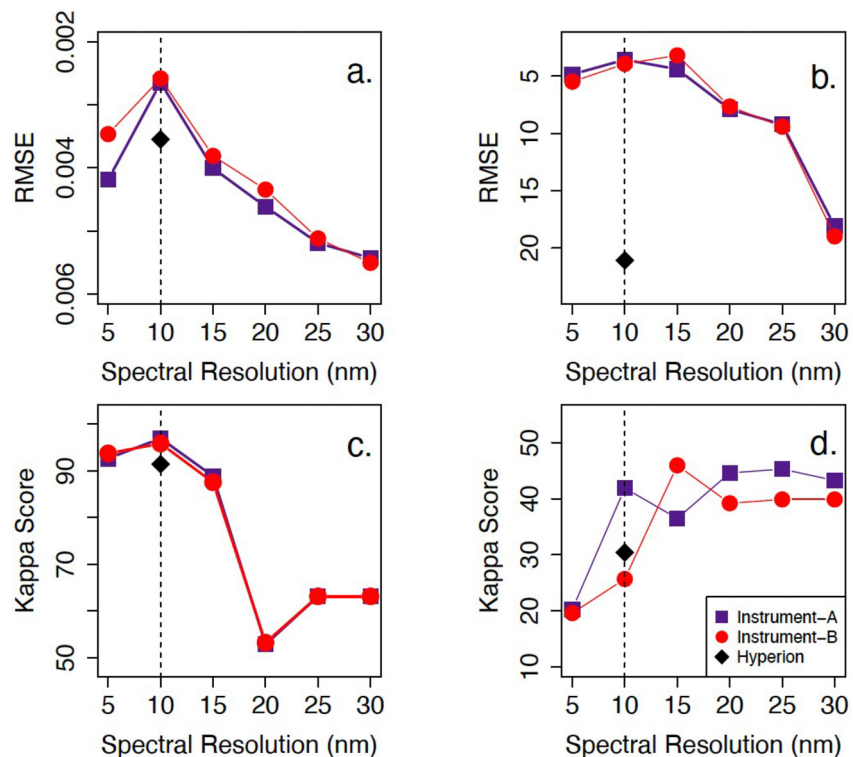


Figure 4. Instrument application algorithm accuracy across spectral resolution colored by scientific area for Instrument-A (purple), Instrument-B (red), and Hyperion (black) for mineral (a), vegetation (b), aquatic (c), and snow (d) retrievals. Root mean square error was calculated for mineral and vegetation spectra while kappa score was calculated for aquatic and snow spectra. Vertical lines represent spectral resolution targets defined by the National Academies' 2018 Decadal Survey on Earth Science and Applications.

experiment incorrectly classified the majority of pixels at low spectral resolutions, classifying all pixels as algae (Figure 4c). This convergence to algae classification caused a dip in the 20 nm spectral resolution experiment).

For the snow algorithm, SNR degraded algorithm accuracy across spectral resolution experiments for both Instrument-A, Instrument-B, and Hyperion (Figure 4d). Approximately 20% of the snow spectra were categorized as having the highest snow grain size in each of the instrument application experiments.

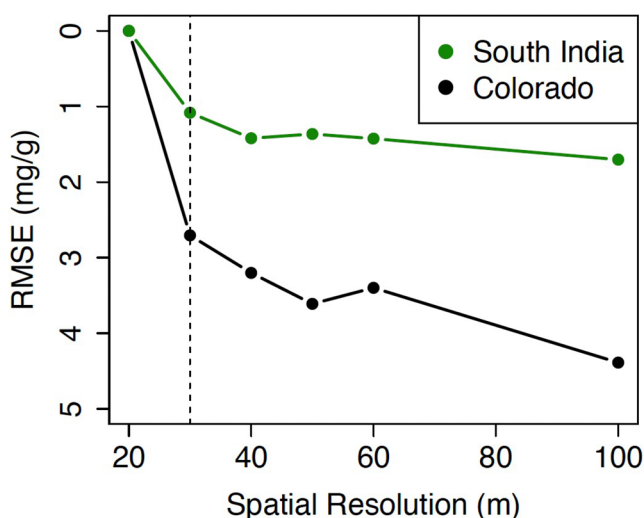


Figure 5. Direct application algorithm accuracy calculated by root mean square error between the degraded resolution and the native resolution across spatial resolution experiments colored by scene. Vertical lines represent spectral resolution targets defined by the National Academies' 2018 Decadal Survey on Earth Science and Applications.

3.2. Spatial Resolution

Retrieval accuracy decreased with coarsening spatial resolutions for both the Colorado and the South India sites in the direct application of the vegetation algorithms. Retrieval accuracy declined more quickly in the heterogeneous Colorado scene than the homogeneous South India scene (black vs. green, Figure 5). The 30 m standard proposed by NASA Earth Science Decadal Survey (2018) provided the most algorithm accuracy across experiments (Figure 5, vertical dotted line). There was a slight increase in retrieval accuracy in the state of Colorado scene between the 50 and 60 m spatial resolution experiments. We assumed this was caused by spectral mixing between vegetated and non-vegetated spectra within a heterogeneous scene.

Instrument-A, Instrument-B, and Hyperion applications that included the effects of noise both greatly decreased retrieval accuracy compared to the direct applications (Figure 6). Increasing SNR over decreasing spatial resolution caused accuracy to increase somewhat for both Instrument-A

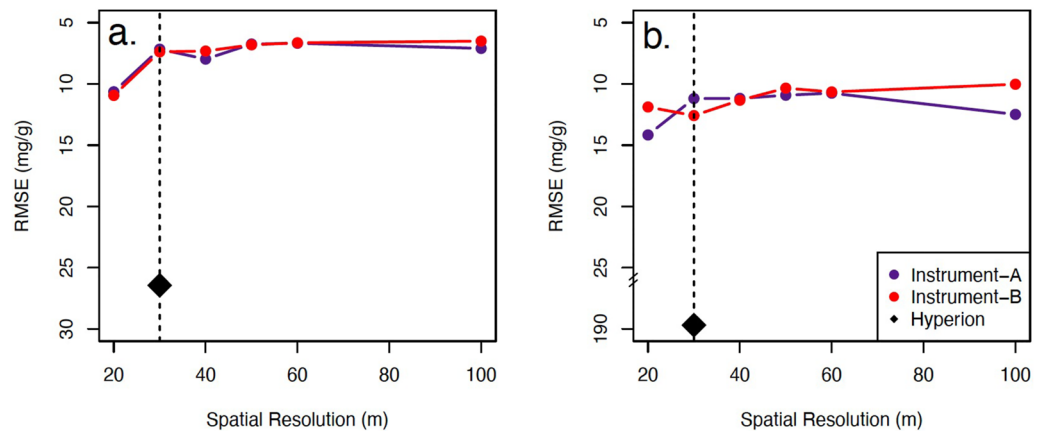


Figure 6. Instrument application algorithm accuracy for South India (a) and Colorado (b) scenes. The instrument application includes the effects of noise on retrieval accuracy while the direct application (Figure 5) does not. Hyperion noise (black diamond) caused large inaccuracy in both vegetation retrievals, but especially in the Colorado scene (b). We have broken the vertical axis to include this point. Vertical lines represent spectral resolution targets defined by the National Academies' 2018 Decadal Survey on Earth Science and Applications.

and Instrument-B applications, especially between 20 and 30 m spatial resolution experiments. Average SNR increased in the SWIR between instruments configured for 20–30 m spatial resolution by 78% SNR for Instrument-A and 81% SNR for Instrument-B (Figure 1, dark purple). Hyperion was most sensitive to the PLSR algorithm (Figure 4b). In comparison to both Instrument-A and Instrument-B, Hyperion poorly estimated canopy nitrogen content.

3.3. Temporal Resolution (Revisit)

Mission revisit cadence greatly affected the probability of detecting short term events (Figure 7). Revisiting more than 20 days for a short-term event (<5 days in duration) resulted in a probability of detection of less than 20%. Long duration events (>21 days in duration) had a higher probability of detection even for greater than 60-day

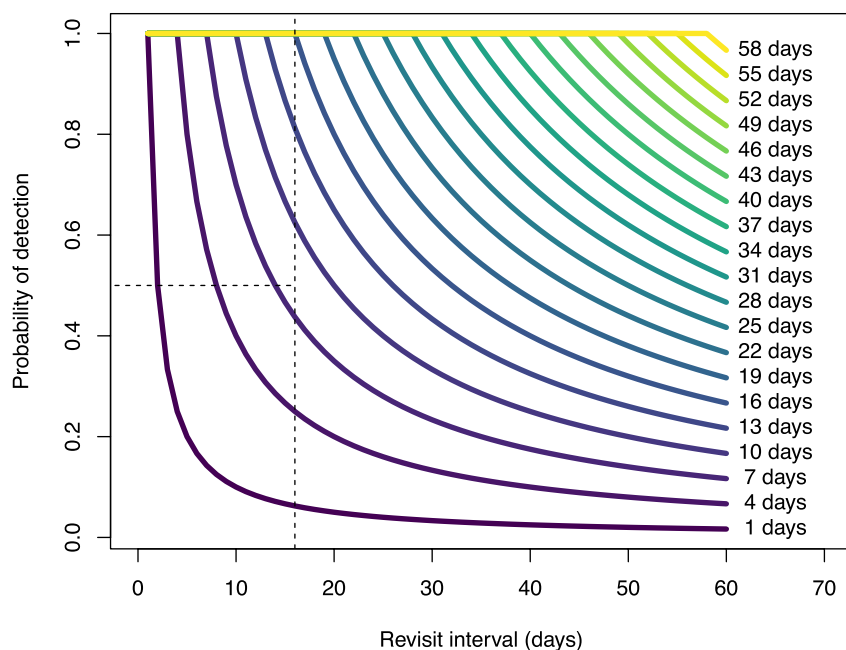


Figure 7. Detection probability as a function of increasing revisit interval colored by the duration of the event where shorter events are more difficult to detect with higher revisit time intervals. The vertical line represents target revisit of 16 days. The horizontal line represents the probability of detection of 0.5 equivalent to a coin flip.

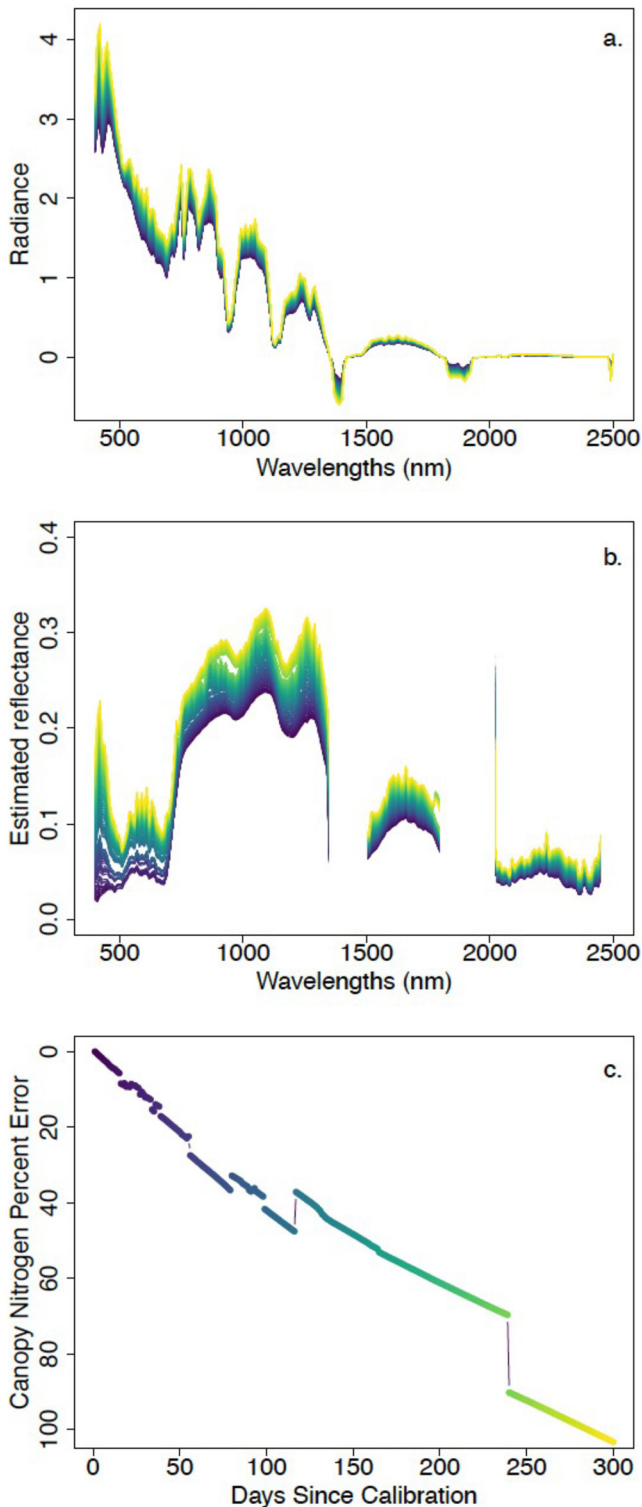


Figure 8. (a) Example radiances with increasing error due to drift or days since calibration. (b) Estimated reflectances of the radiances in (a). (c) canopy nitrogen percent error as a function of days since calibration. Colors in a, b, and c correspond to days since calibration.

revisits (probability >40%). Lastly, calibration drift decayed retrieval accuracy (Figure 8). Percent error reached 60% in 175 days since calibration and 100% in 300 days since calibration.

4. Discussion

Accurate retrieval of Earth's geophysical properties from imaging spectroscopy requires advanced mission planning based on scientific evaluation to meet the requirements of multiple scientific areas. This suite of driving cases covers three aspects (i.e., spectral, spatial, and revisit) of mission architecture interlinked with SNR and four of the five core science areas, showing where high-resolution requirements are necessary to preserve algorithm accuracy. Our analyses confirm that high spectral (~10 nm), high spatial (~30 m), and high revisit (less than 16 days) design is needed to effectively quantitatively constrain Earth's geophysical property estimation with hyperspectral imagery and corresponding retrieval algorithms. These mission design choices are currently used in the German spaceborne imaging spectrometer mission called the Environmental Mapping and Analysis Program (i.e., EnMap; 10 nm, 30 m, 4 days; Guanter et al., 2015). We represent these targets (i.e., 10 nm, 30 m, and <16 days) with Figures 3–7 vertical dotted lines. Specifically, instruments with a spatial resolution of 30 m and a spectral resolution of 10 nm obtain the largest accuracies, across the five scientific foci explored here. Furthermore, the probability of detection for short-term events (i.e., event duration < 7 days) was less than 0.5 for revisit intervals 16 days and longer (Figure 7). This largely corroborates the performance proposed by the Decadal Survey in their original description of the SBG mission concept. We also highlight the difference between instrument choices Instrument-A and Instrument-B and past instrument Hyperion to showcase how the instrument selection process may be informed by simulation experiments using hypertrace or similar mission design workflows. Overall, the instruments performed similarly and outperformed Hyperion (see Figures 4 and 6). In the following paragraphs, we elaborate on our findings for each type of resolution and finally describe our vision for the future of NASA mission architecture studies.

We build upon previous research on mineral and vegetation retrieval algorithms (Kokaly et al., 2009; Shiklomanov et al., 2016; Swayze et al., 2003) showing that high spectral resolution (~10 nm) improved retrieval estimation across all scientific areas (Figure 3). In our mineral assessment, we used Kaolinite absorption feature matching. This retrieval algorithm depends on a narrow range of wavelengths (i.e., 2100–2300 nm). As the spectral resolution is coarsened, the number of data points within this range decreases rapidly and results in an exponential loss of information over spectral resolution. Similarly, least squares spectral matching uses a spectral library as a reference for determining the amount of snow in a pixel (Dozier & Painter, 2004). Aquatic benthic cover classification and vegetation PLSR algorithms use coefficients that are empirically estimated using in situ and concurrently measured hyperspectral data, and are then applied to remotely sensed imaging spectrometer data (Cawse-Nicholson et al., 2019; Serbin & Townsend, 2020; Thompson, Hochberg, et al., 2017). The in situ data are collected at particular spectral and spatial resolutions at specific locations usually during the summer months with both airborne and field data, which may ultimately drive the sensitivity of these algorithms to degrading spectral resolution (e.g., Hochberg and Atkinson, 2003). More work is needed to understand what the optimal sampling scheme is

for both in situ and remotely sensed hyperspectral data and how to use these data in tandem for improving aquatic classifications and vegetation trait estimation algorithm retrievals. For instance, our work suggests that ever-increasing the spectral resolution of an imaging spectrometer may be ill-advised given the tradeoffs between SNR and spectral resolution (Figure 1). Similarly, temporal resolution analysis (Figure 7) suggests that to capture short-duration events, like phenological changes in vegetation, higher revisit both in the field and air may be more important than higher spectral or spatial resolutions. In order to understand the optimal sampling scheme, more collocated studies with longer time series of paired field data and hyperspectral imagery must be performed.

Increased spatial resolution is a particularly important component for vegetation research because plants operate on individual plant scales and aggregate and interact at the ecosystem scale to drive Earth system level phenomena (e.g., an individual spruce tree to the boreal forest). Earth system scientists are increasingly arguing for representing cohorts or individual-level plant traits and processes at a large scale to inform Earth system models (Fisher et al., 2018). SBG would greatly influence these models by providing a large-scale data set at a relevant level of plant organization (i.e., ~30 m; Turner et al., 2019). We show (Figure 4) a quantitative threshold for spatial resolution from the vegetation algorithm perspective. However, both mission and instrument design must be carefully constructed to include high spatial resolution and accommodate physical barriers that may decrease the SNR. For the same instrument and global coverage, narrower swath/field-of-view means better spatial resolution and more consistent angular sampling but worse temporal resolution. So, an advance in spatial resolution may mean compromising in temporal resolution. Coordinated international collaborations with other global imaging spectroscopy missions (e.g., European Space Agency's Copernicus Hyperspectral Imaging Mission) might provide a path forward for meeting high revisit science requirements while also improving spatial resolution. Future work may focus on understanding how high spatial resolution multispectral imagery could inform lower spatial resolution hyperspectral trait estimation to ultimately improve global vegetation trait data. Gap-filling approaches have been used to increase spectral and temporal resolutions of multi-spectral imagery (e.g., Moreno-Martinez et al., 2020). Concurrent hyperspectral and multispectral imagery will improve the accuracy of gap-filling approaches by providing spectral validation data sets and may allow for spectral data imputation of past multi-spectral imagery thus increasing temporal resolution of hyperspectral imagery. Similarly, the higher spatial resolution multi-spectral instruments may allow for improved analysis of lower spatial resolution hyperspectral images by informing the mixture components of the spectral signals in the hyperspectral image which would provide a higher sample size of multi-spectral signatures within a hyperspectral pixel.

Altering the orbiting altitude of an instrument with a particular spatial resolution configuration can increase SNR by allowing more photons to be received from a particular pixel. But a particular orbiting altitude with longer revisit intervals may not be desirable for short duration event detection (Figure 6, dark purple). While our assessment relies on simulated data, increased revisit will increase the probability that events such as volcanic eruptions or mudslides are detected by SBG. Extreme events are increasing with frequency as the climate changes (NASA ESAS, 2016) and the effects of these types of events may be some of the most important aspects of mission design to the public. Furthermore, our analysis is optimistic as it did not include a source of clouds where the presence of clouds will lead to missing data and in turn longer revisit. Higher revisit will enable a higher probability that any image is taken because it will be more likely that an overpass occurs on a clear or semi-clear day. While satellite constellations may help improve the revisit interval, the calibration drift greatly affects retrieval accuracy (Figure 8) and would need to be included in the uncertainty propagation of retrievals from satellite constellations.

The SBG mission is driven by the ideals of the decadal survey, striving to better understand the changing geophysical properties across the Earth system (National Academies of Sciences, Engineering, and Medicine, 2018). We have shown the dominant components that drive retrieval uncertainty across four core scientific areas. Our approach utilizes a workflow for simulating the SNR effects of mission instruments and includes many aspects of data processing uncertainties. Future work may focus on using this type of setup for mission planning where simulations may be run to parse out different dominant contributors of uncertainty. For example, intrinsic dimensionality can provide an algorithm agnostic evaluation approach by focusing simply on information content (Cawse-Nicholson et al., 2019). Once the mission design has been finalized our method can be used to inform the data pipeline from SBG or future hyperspectral missions by applying realistic uncertainties along the data processing steps and ultimately improve biogeoscience with more accurate geophysical property estimation.

Data Availability Statement

The data used in this work are hyperspectral images collected from past published works (listed in Table 1). The software used in this work is ISOFIT (<https://doi.org/10.5281/ZENODO.4614338>), HYPERTRACE (<https://github.com/isofit/isofit/tree/master/examples/py-hypertrace>), and four types of hyperspectral algorithms (see Table 1).

Acknowledgments

Some of the research described in this paper was carried out at the Jet Propulsion Laboratory, California Institute of Technology, under contract with the National Aeronautics and Space Administration. Government sponsorship acknowledged. We acknowledge funding from NASA's Surface Biology and Geology Designated Observable. S.P.S. was also supported by the United States Department of Energy contract no. DE-SC0012704 to Brookhaven National Laboratory and the National Aeronautics and Space Administration Surface Biology and Geology (SBG) mission study (80GSFC22TA016).

References

- Bioucas-Dias, J. M., & Nascimento, J. M. P. (2005). Estimation of signal subspace on hyperspectral data. In L. Bruzzone (Ed.) (p. 59820L). *Proc. SPIE 5982, Image and Signal Processing for Remote Sensing XI*. <https://doi.org/10.1117/12.620061>
- Burnett, A. C., Anderson, J., Davidson, K. J., Ely, K. S., Lamour, J., Li, Q., et al. (2021). A best-practice guide to predicting plant traits from leaf-level hyperspectral data using partial least squares regression. *Journal of Experimental Botany*, *72*(18), 6175–6189. <https://doi.org/10.1093/jxb/erab295>
- Cause-Nicholson, K., Hook, S. J., Miller, C. E., & Thompson, D. R. (2019). Intrinsic dimensionality in combined visible to thermal infrared imagery. *IEEE Journal of Selected Topics in Applied Earth Observations and Remote Sensing*, *12*(12), 4977–4984. <https://doi.org/10.1109/JSTARS.2019.2938883>
- Cause-Nicholson, K., Townsend, P. A., Schimel, D., Assiri, A. M., Blake, P. L., Buongiorno, M. F., et al. (2021). NASA's surface biology and geology designated observable: A perspective on surface imaging algorithms. *Remote Sensing of Environment*, *257*, 112349. <https://doi.org/10.1016/j.rse.2021.112349>
- Chadwick, K. D., Brodrick, P. G., Grant, K., Goulden, T., Henderson, A., Falco, N., et al. (2020). Integrating airborne remote sensing and field campaigns for ecology and Earth system science. *Methods in Ecology and Evolution*, *11*(11), 1492–1508. <https://doi.org/10.1111/2041-210X.13463>
- Committee on Extreme Weather Events and Climate Change Attribution, Board on Atmospheric Sciences and Climate, Division on Earth and Life Studies, & National Academies of Sciences, Engineering, and Medicine. (2016). *Attribution of extreme weather events in the context of climate change*. National Academies Press. <https://doi.org/10.17226/21852>
- Connelly, D. S., Thompson, D. R., Mahowald, N. M., Li, L., Carmon, N., Okin, G. S., & Green, R. O. (2021). The EMIT mission information yield for mineral dust radiative forcing. *Remote Sensing of Environment*, *258*, 112380. <https://doi.org/10.1016/j.rse.2021.112380>
- Curran, P. J. (1989). Remote sensing of foliar chemistry. *Remote Sensing of Environment*, *30*(3), 271–278. [https://doi.org/10.1016/0034-4257\(89\)90069-2](https://doi.org/10.1016/0034-4257(89)90069-2)
- Dietersen, H. M. (2021). Corrigendum: Hyperspectral measurements, parameterizations, and atmospheric correction of whitecaps and foam from visible to shortwave infrared for ocean color remote sensing. *Frontiers of Earth Science*, *9*, 683136. <https://doi.org/10.3389/feart.2021.683136>
- Dozier, J., & Painter, T. H. (2004). Multispectral and hyperspectral remote sensing of alpine snow properties. *Annual Review of Earth and Planetary Sciences*, *32*(1), 465–494. <https://doi.org/10.1146/annurev.earth.32.101802.120404>
- Fisher, R. A., Koven, C. D., Anderegg, W. R., Christoffersen, B. O., Dietze, M. C., Farris, C. E., et al. (2018). Vegetation demographics in Earth system models: A review of progress and priorities. *Global Change Biology*, *24*(1), 35–54. <https://doi.org/10.1111/gcb.13910>
- García, R. A., Lee, Z., Barnes, B. B., Hu, C., Dietersen, H. M., & Hochberg, E. J. (2020). Benthic classification and IOP retrievals in shallow water environments using MERIS imagery. *Remote Sensing of Environment*, *249*, 112015. <https://doi.org/10.1016/j.rse.2020.112015>
- German Aerospace Center (DLR). (2019). DESIS - Hyperspectral Images - Global. <https://doi.org/10.15489/hxom21uqeo90>
- Guanter, L., Kaufmann, H., Segl, K., Foerster, S., Rogass, C., Chabrillat, S., et al. (2015). The EnMAP spaceborne imaging spectroscopy mission for Earth observation. *Remote Sensing*, *7*(7), 8830–8857. <https://doi.org/10.3390/rs70708830>
- Hochberg, E. J., & Atkinson, M. J. (2003). Capabilities of remote sensors to classify coral, algae, and sand as pure and mixed spectra. *Remote Sensing of Environment*, *85*(2), 174–189. [https://doi.org/10.1016/S0034-4257\(02\)00202-X](https://doi.org/10.1016/S0034-4257(02)00202-X)
- Hu, C. (2011). An empirical approach to derive MODIS ocean color patterns under severe sun glint. *Geophysical Research Letters*, *38*(1). <https://doi.org/10.1029/2010GL045422>
- Isokit, Brodrick, P. I., Erickson, A., Jfahlen, Winstonolson, Thompson, D. R., et al. (2021). *isofit/isofit: 2.8.0 (Version v2.8.0)*. Zenodo. <https://doi.org/10.5281/ZENODO.4614338>
- Kokaly, R. F., Asner, G. P., Ollinger, S. V., Martin, M. E., & Wessman, C. A. (2009). Characterizing canopy biochemistry from imaging spectroscopy and its application to ecosystem studies. *Remote Sensing of Environment*, *113*, S78–S91. <https://doi.org/10.1016/j.rse.2008.10.018>
- Moreno-Martínez, A., Izquierdo-Verdiguier, E., Maneta, M. P., Camps-Valls, G., Robinson, N., Muñoz-Marí, J., et al. (2020). Multispectral high resolution sensor fusion for smoothing and gap-filling in the cloud. *Remote Sensing of Environment*, *247*, 111901. <https://doi.org/10.1016/j.rse.2020.111901>
- National Academies of Sciences, Engineering, and Medicine (U.S.), National Academies of Sciences, Engineering, and Medicine (U.S.), & National Academies of Sciences, Engineering, and Medicine (U.S.). (2018). In *Thriving on our changing planet: A decadal strategy for Earth observation from space*. The National Academies Press.
- Nolin, A. W., & Dozier, J. (1993). Estimating snow grain size using AVIRIS data. *Remote Sensing of Environment*, *44*(2–3), 231–238. [https://doi.org/10.1016/0034-4257\(93\)90018-S](https://doi.org/10.1016/0034-4257(93)90018-S)
- Schaepman-Strub, G., Schaepman, M. E., Painter, T. H., Dangel, S., & Martonchik, J. V. (2006). Reflectance quantities in optical remote sensing—Definitions and case studies. *Remote Sensing of Environment*, *103*(1), 27–42. <https://doi.org/10.1016/j.rse.2006.03.002>
- Schimel, D., Townsend, P. A., & Pavlick, R. (2020). Prospects and pitfalls for spectroscopic remote sensing of biodiversity at the global scale. In J. Cavender-Bares, J. A. Gamon, & P. A. Townsend (Eds.), *Remote sensing of plant biodiversity* (pp. 503–518). Springer International Publishing.
- Serbin, S. P., & Townsend, P. A. (2020). Scaling functional traits from leaves to canopies. In *Remote sensing of plant biodiversity* (pp. 43–82). Springer.
- Shiklomanov, A. N., Dietze, M. C., Viskari, T., Townsend, P. A., & Serbin, S. P. (2016). Quantifying the influences of spectral resolution on uncertainty in leaf trait estimates through a Bayesian approach to RTM inversion. *Remote Sensing of Environment*, *183*, 226–238. <https://doi.org/10.1016/j.rse.2016.05.023>
- Skiles, S. M., & Painter, T. (2017). Daily evolution in dust and black carbon content, snow grain size, and snow albedo during snowmelt, Rocky Mountains, Colorado. *Journal of Glaciology*, *63*(237), 118–132. <https://doi.org/10.1017/jog.2016.125>

- Stavros, E. N., Chrono, J., Cawse-Nicholson, K., Freeman, A., Glenn, N. F., Guild, L., et al. (2023). Designing an observing system to study the surface biology and geology (SBG) of the Earth in the 2020s. *Journal of Geophysical Research: Biogeosciences*, 128(1), e2021JG006471. <https://doi.org/10.1029/2021JG006471>
- Swayze, G. A. (2003). Effects of spectrometer band pass, sampling, and signal-to-noise ratio on spectral identification using the Tetracorder algorithm. *Journal of Geophysical Research*, 108(E9), 5105. <https://doi.org/10.1029/2002JE001975>
- Swayze, G. A., Clark, R. N., Goetz, A. F. H., Livo, K. E., Breit, G. N., Kruse, F. A., et al. (2014). Mapping advanced Argillic Alteration at Cuprite, Nevada, using imaging spectroscopy. *Economic Geology*, 109(5), 1179–1221. <https://doi.org/10.2113/econgeo.109.5.1179>
- Thompson, D. R., Bearden, D., Brosnan, I., Cawse-Nicholson, K., Chrono, J., Green, R. O., et al. (2021). NASA's surface biology and geology concept study: Status and next steps. In *2021 IEEE International Geoscience and Remote Sensing Symposium IGARSS* (pp. 112–114). IEEE. <https://doi.org/10.1109/IGARSS47720.2021.9554480>
- Thompson, D. R., Boardman, J. W., Eastwood, M. L., & Green, R. O. (2017). A large airborne survey of Earth's visible-infrared spectral dimensionality. *Optics Express*, 25(8), 9186. <https://doi.org/10.1364/OE.25.009186>
- Thompson, D. R., Hochberg, E. J., Asner, G. P., Green, R. O., Knapp, D. E., Gao, B.-C., et al. (2017). Airborne mapping of benthic reflectance spectra with Bayesian linear mixtures. *Remote Sensing of Environment*, 200, 18–30. <https://doi.org/10.1016/j.rse.2017.07.030>
- Thompson, D. R., Natraj, V., Green, R. O., Helmlinger, M. C., Gao, B.-C., & Eastwood, M. L. (2018). Optimal estimation for imaging spectrometer atmospheric correction. *Remote Sensing of Environment*, 216, 355–373. <https://doi.org/10.1016/j.rse.2018.07.003>
- Turner, D. J., Malenovsky, Z., Lucieer, A., Turnbull, J. D., & Robinson, S. A. (2019). Optimizing spectral and spatial resolutions of unmanned aerial system imaging sensors for monitoring Antarctic vegetation. *IEEE Journal of Selected Topics in Applied Earth Observations and Remote Sensing*, 12(10), 3813–3825. <https://doi.org/10.1109/JSTARS.2019.2938544>
- Turner, M. G., Dale, V. H., & Gardner, R. H. (1989). Predicting across scales: Theory development and testing. *Landscape Ecology*, 3(3–4), 245–252. <https://doi.org/10.1007/BF00131542>
- Vermote, E. F., & Kotchenova, S. (2008). Atmospheric correction for the monitoring of land surfaces. *Journal of Geophysical Research*, 113(D23), D23S90. <https://doi.org/10.1029/2007JD009662>
- Verrelst, J., Malenovsky, Z., Van der Tol, C., Camps-Valls, G., Gastellu-Etchegorry, J.-P., Lewis, P., et al. (2019). Quantifying vegetation biophysical variables from imaging spectroscopy data: A review on retrieval methods. *Surveys in Geophysics*, 40(3), 589–629. <https://doi.org/10.1007/s10712-018-9478-y>
- Wang, R., Gamon, J. A., Cavender-Bares, J., Townsend, P. A., & Zygielbaum, A. I. (2018). The spatial sensitivity of the spectral diversity–biodiversity relationship: An experimental test in a prairie grassland. *Ecological Applications*, 28(2), 541–556. <https://doi.org/10.1002/eap.1669>
- Zheng, T., Singh, A., Desai, A. R., Krishnayya, N. K., & Townsend, P. A. (2023). Variability in forest plant traits along the Western Ghats of India and their environmental drivers at different resolutions. bioRxiv. <https://doi.org/10.1101/2023.02.01.526666>